

A unified model for the speed of sound in cranial bone based on genetic algorithm optimization

Christopher W Connor^{1,2}, Greg T Clement¹ and Kullervo Hynynen¹

¹ Brigham & Women's Hospital, Harvard Medical School, 221 Longwood Avenue, Boston, MA 02115, USA

² Massachusetts Institute of Technology, 77 Massachusetts Avenue, Cambridge, MA 02139, USA

Received 4 July 2002

Published 28 October 2002

Online at stacks.iop.org/PMB/47/3925

Abstract

The density and structure of bone is highly heterogeneous, causing wide variations in the reported speed of sound for ultrasound propagation. Current research on the propagation of high intensity focused ultrasound through an intact human skull for non-invasive therapeutic action on brain tissue requires a detailed model for the acoustic velocity in cranial bone. Such models have been difficult to derive empirically due to the aforementioned heterogeneity of bone itself.

We propose a single unified model for the speed of sound in cranial bone based upon the apparent density of bone by CT scan. This model is based upon the coupling of empirical measurement, theoretical acoustic simulation and genetic algorithm optimization. The phase distortion caused by the presence of skull in an acoustic path is empirically measured. The ability of a theoretical acoustic simulation coupled with a particular speed-of-sound model to predict this phase distortion is compared against the empirical data, thus providing the fitness function needed to perform genetic algorithm optimization. By performing genetic algorithm optimization over an initial population of candidate speed-of-sound models, an ultimate single unified model for the speed of sound in both the cortical and trabecular regions of cranial bone is produced.

The final model produced by genetic algorithm optimization has a nonlinear dependency of speed of sound upon local bone density. This model is shown by statistical significance to be a suitable model of the speed of sound in bone. Furthermore, using a skull that was not part of the optimization process, this model is also tested against a published homogeneous speed-of-sound model and shown to return an improved prediction of transcranial ultrasound propagation.

(Some figures in this article are in colour only in the electronic version)

1. Introduction

Focused ultrasound provides a non-invasive method for inducing temperature elevations in tumours (Fry and Johnson 1978, Lele and Pierce 1973, Lizzi *et al* 1984, Chapelon *et al* 1993, Sanghvi *et al* 1996, ter Haar *et al* 1989), resulting in the coagulation of the tumour. It has long been recognized that the ability to produce a high intensity ultrasound focus within the brain, and hence non-invasive cautery at that focus due to acoustic absorption by brain tissue, would provide a minimally invasive means of treating deep-seated brain tumours without disturbing overlying structures (Fry *et al* 1954, Lele 1967). It is clearly desirable to produce this focus through an intact skull rather than requiring craniotomy to establish an acoustic window, which has led to interest in the study of the propagation of ultrasound through the bones of the skull (Sun and Hynynen 1998, Hynynen and Jolesz 1998, Tanter *et al* 1998). Although bone in general was first considered to be an impassible barrier to therapeutic ultrasound, and was then considered to induce too much distortion into the acoustic field to allow a therapeutic focus to be formed (Lynn *et al* 1942, Lynn and Putnam 1944), simulation and experimental studies have since shown that a therapeutic focus may be formed inside an intact skull if suitable phase compensations are applied over the ensonicating field by means of a segmented transducer (Hynynen and Jolesz 1998, Sun and Hynynen 1999).

An entirely non-invasive therapeutic ultrasound system using transcranial focusing clearly requires that the appropriate phase corrections be determined non-invasively (Hynynen 1999). Acoustic simulation can be utilized to determine the distortion an intact skull would introduce into an incident uniform ultrasound field, and hence to determine the appropriate phase compensations to reverse this distortion (Clement and Hynynen 2002a). Potentially, many different acoustic simulation techniques may be applied to this problem, including acoustic time reversal, inversion of linear filters, inversion of Helmholtz operators, Rayleigh–Sommerfield analysis, and formulations such as KZK and linear or nonlinear finite-difference time-domain (FDTD) (Tanter *et al* 2001, Greenleaf 1986, Averkiou and Cleveland 1999, Hallaj and Cleveland 1999). These simulations are based on the reconstruction of CT data to provide the geometry and composition of each individual skull (Clement and Hynynen 2002a). CT data in Hounsfield units (HUs) may be readily normalized to apparent density by ensuring that materials of known density are included in the scan.

The field correction calculations under all these simulation methods are dependent on the velocity with which the ultrasound is propagated through the skull. However, skull is a heterogeneous material, so it does not have a single speed of sound throughout. Furthermore, its heterogeneity makes it difficult to determine empirically what the variation in speed of sound throughout a sample of skull might be. This difficulty is reflected in the literature on the material properties of the skull: estimates of the speed of sound in skull are given as speed of sound through some bulk sample of skull bone, referred to as the plesiovelocity (Lees *et al* 1979). Especially, the consensus across the literature is not convincing. A common approach to attempt to improve on these circumstances is to divide the skull into a three-layer model (Fry and Barger 1978), comprising an inner and outer table of cortical bone between which trabecular bone is sandwiched. This distinction into layers is somewhat arbitrary since much skull bone is of an intermediate porosity and hence is not robustly assignable to either category. Sharp divisions between the three layers are similarly seen to be lacking in anatomical specimens.

Hence, we find ourselves in the situation of requiring a functional model of local speed of sound in bone based on the apparent bone density at a particular point, but seemingly confounded from producing such a model empirically due to the high variability of the material under study. We propose that this problem may be made tractable by using an empirical

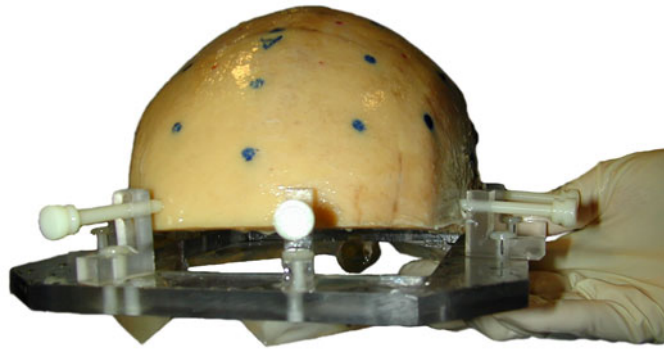


Figure 1. A human calvarium mounted in a stereotactic positioning frame.

acoustic approach combined with the genetic algorithm optimization (Holland 1975) of a population of candidate functions relating apparent bone density to local speed of sound.

2. Method

2.1. Overview

The acoustic properties of a material in bulk may be measured by examining the transmission of ultrasound through a sample of that material, and this technique may be used to examine the bulk properties of a heterogeneous material such as bone (Lakes *et al* 1985). In this study, we concentrate on the phase difference between the received wave and the transmitted wave in continuous wave sonication. In particular, we examine the change in this phase difference between the case where only degassed water is present between the transducer and receiver, and the case where a human calvarium is placed between the transducer and the receiver.

The human calvaria used empirically above are first CT scanned at high clinical resolution. Once the overall geometric structure and the density distribution of the calvaria have been acquired, the experiment described above can be reproduced as a computational simulation of acoustic propagation. The change in phase difference measurement described above is calculated for the simulation. This measurement is acutely sensitive to the speed of sound in the bone. The problem then becomes one of optimizing the model used for speed of sound in bone in the simulation.

This optimization problem is ideally suited to treatment with a genetic algorithm since there is a well-defined, quantifiable success function, which is the total deviation of the simulated phases from the empirical phases. Furthermore, the genetic algorithm optimization technique does not depend on gradient information that may be unacceptably noisy since it would only be available by numerical approximation in this case. This optimization method is also relatively insensitive to local minima and maxima. The genetic algorithm optimization technique can be easily tailored to known physical constraints such that only physically realistic models are permitted (Poloni and Pediroda 1998).

2.2. Empirical configuration

The calvaria were maintained in wet condition so that their acoustic properties remain comparable to *in vivo* bone. The CT scan was performed using a Siemens Somatom Plus 4 with deconvolution kernel AH-82. The calvaria were placed within stereotactic frames as shown in figure 1 to allow their accurate positioning during both the experimental procedure

and CT scanning. Fiducial markers on the frame allow the position and orientation of the skull during the experimental procedure to be accurately matched to a solid body geometric transformation of the reconstructed data.

Ultrasound sonication was performed in degassed, deionized, room-temperature water at 0.74 MHz, which is within the acoustic window for skull bone (Fry 1979) while being of an appropriate frequency for the accurate measurement of the phase component. While an increase in temperature in cranial bone may produce changes in the phase of the received ultrasound wave (Clement and Hynynen 2002b), the amplitude and duration of the sonication used here are such that no appreciable change in skull temperature occurs during measurement.

A 500-element hemispherical ultrasound transducer was used to provide ultrasound transmitters. Forty transducer elements were selected at random from the 500 total elements. These elements were activated in turn while a 0.2 mm diameter polyvinylidene difluoride (PVDF) hydrophone (Precision Acoustics, UK) located at the geometric centre of the hemispherical transducer by a three-dimensional (3D) stepper motor positioning system (Parker, Hannifin, Pennsylvania) was used as the receiver. This allowed the rapid assaying of 40 different acoustic paths through a particular calvarium. The phase information for each acoustic path was acquired automatically using a pre-amp (Precision Acoustics, UK) recorded by digital GPIB IEEE-488 compliant oscilloscope (Textronix, Oregon, Model 380). The empirical experimental design here is similar to that used in Clement and Hynynen (2002a).

2.3. Genetic algorithm representation

A model for speed of sound in bone can be determined by admitting an initial large pool of candidate speed-of-sound models, and ascertaining how well these simulations predict the phase changes as established by empirical study. These speed-of-sound models are then used to produce a new generation of speed-of-sound models that are similarly studied. However, it is required that these speed-of-sound models be stated in a form amenable to manipulation by genetic algorithms.

Bone may be considered to be a composite of inorganic mineral within an organic framework. The mineral component is predominantly hydroxyapatite, which may be present in a crystalline form with a density of up to 3170 kg m^{-3} (Katz 1971). Type I collagen contributes 90% of the organic material and, like most organic materials, has a density similar to that of water (Lees 1986). The speed of sound in skull in bulk has not been reported to be greater than 3500 m s^{-1} . The fastest reported speed of sound for bulk ultrasonic propagation in wet non-dental bone is 4180 m s^{-1} (Lees *et al* 1983), which was seen in cow tibia. Faster speeds of sound are possible in dry bone as the collagen matrix stiffens, but this is not representative of the *in vivo* case.

The genetic algorithm representation of the speed function is as five 'knots' arranged on a graph with densities between 1000 and 3400 kg m^{-3} , and speeds of sound between 1500 and 5500 m s^{-1} . The speed of sound and density of water establish the lower bounds. The upper bound is set slightly above the maximum possible density of 3170 kg m^{-3} ; optimization techniques may perform poorly if the maximum of the optimization is located in a corner of the search space, and this small margin potential alleviates that risk. The maximum speed of sound is set higher than the reported maximum speed of sound, not only to aid the optimization process but also because the reported maximum speed of sound above is given as a bulk property and we must allow for the possibility that the speed of sound in some small portion of the tissue may be much higher.

The continuous model of the speed of sound can now be represented in the discrete allelic form required for this method of optimization (Poloni and Pediroda 1998, Shaffer and Small

1996). The function $c(\rho)$, the model speed of sound dependent on the local apparent bone density, is generated from these allelic knots by minimizing (De Boor 1978)

$$\nu \cdot \sum_{i=1}^5 [c_i - c(\rho_i)]^2 + (1 - \nu) \cdot \int_{1000}^{3400} \left(\frac{d^2c}{d\rho^2} \right)^2 d\rho \tag{1}$$

where c_i and ρ_i are the allelic knots, and ν is a numeric value between 0 and 1 that balances the relative importance of fitting the knots closely with the requirement that the function $c(\rho)$ be reasonably smooth. This operation is part of the class of cubic smoothing splines. This avoids the well-known problem with polynomial function fitting where the knots are perfectly fit but the function displays unacceptable hilliness in between the knots. Selecting a value of $\nu = 0.99$ places strong emphasis on fitting the knots (the first part of the equation) while providing acceptably smooth and responsive fitting in the regions between.

Functions that are not monotonically increasing or nearly so are discarded as unacceptable genetic forms: all functions must satisfy the admissibility equation (2) where $c_{\text{tolerance}}$ is set to 200 m s^{-1} ,

$$c(\rho_0) + c_{\text{tolerance}} \geq \max_{1000 < \rho < \rho_0} (c(\rho)) \quad 1000 < \rho_0 \leq 3400. \tag{2}$$

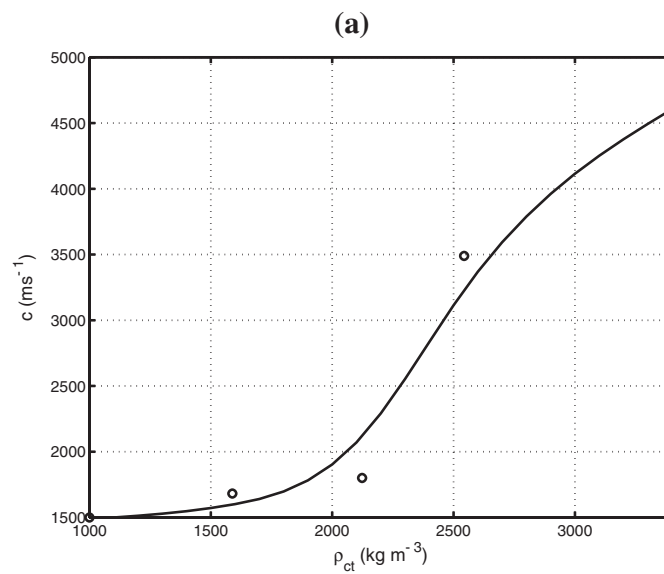
In optimization by genetic algorithm, it is important to allow a certain level of tolerance in enforcing limits such as these so that potentially useful genetic alleles are not entirely discarded out of hand. Curves such as those shown in figure 2 are representative of the types of speed-of-sound models simulated.

A quantitative success function is required to measure the fitness of each particular speed-of-sound model. A parameter θ_e is calculated for each acoustic path; this is the error between the phase change as calculated by the simulation and the phase change as measured empirically. The success function is then defined as $\overline{\cos \theta_e} \times 100\%$, i.e., the arithmetic mean of the cosines of the θ_e distribution as a percentage. The success function has a range of 100% for a perfect correlation down to -100% for a perfect anti-correlation; the success function is a phase correlation metric.

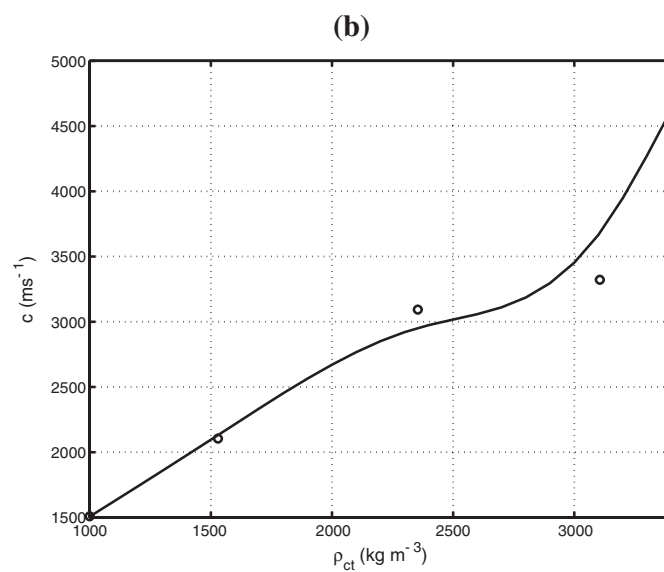
The alleles are stored as floating point numbers as shown in figure 2, hence the genetic algorithm is of the real-coded type. Most original work on the robustness of genetic algorithms was performed on binary-coded algorithms. However, by extension of the demonstration of the robustness of genetic algorithms over non-binary alphabets (Antonisse 1989), real-coded algorithms have also been shown to perform in accordance with Holland’s schemata (Holland 1975, Wright 1991).

Each generation of models is evolved from the previous one by the three steps of competitive tournament selection, breeding based on allelic crossover, and the application of a low rate of spontaneous mutation (Goldberg and Deb 1991).

Firstly, the tournament selection step is performed by selecting two models at random from the current population. Of these two models, the one that produced the best score using the success function is allowed to form part of the breeding pool that produces the next generation. Models chosen in this way are not removed from the current population. This produces a breeding pool that is guaranteed not to contain the worst performing model from the current population, and should also favour the inclusion of better performing models. This selection method has two further useful properties. It has limited susceptibility to being overwhelmed early in the optimization process by a single highly successful model, which can cause problems in genetic algorithm optimization due to loss of population diversity. This selection method also is not dependent on the absolute value returned by the success function and simulation method, but only on the relative value of the success function between models: thus in this case, the only requirement is that a better speed-of-sound model should



ρ_{ct}	1000.0	1588.5	2123.2	2543.4	3400.0
c	1500.0	1681.5	1799.9	3489.7	4566.4



ρ_{ct}	1000.0	1529.3	2354.4	3106.0	3400.0
c	1509.1	2105.4	3093.7	3322.3	4864.9

Figure 2. Examples from the population of potential speed-of-sound models.

generally produce a better result in the success function. In practice, this means that the success function can exhibit nonlinear or noisy behaviour without adversely disturbing the optimization process.

Secondly, two parent models are selected at random from the breeding pool, and a new child model is produced from this pair and becomes a member of the next generation. Eighty per cent of the time, this new child model is produced by selecting a random point in its alleles and including the alleles of the first parent model up to that point, and the alleles of the second parent model after that point; this is known as allelic crossover. Twenty per cent of the time, the child model is a direct copy of a parent. This tends to allow successful models to propagate through to the next generation.

Thirdly, 10% of the time a random mutation is added to the alleles of a particular model, with a permissible mutation range of $\pm 200 \text{ kg m}^{-3}$ and $\pm 200 \text{ m s}^{-1}$. While this mutation rate would be high for binary-coded algorithms where a single bit mutation can produce a huge variation in the numerical value it represents, it is appropriate for real-coded genetic algorithms, which are more robust in this sense.

Any models in this new generation that are not physically valid by the criteria given above are deleted, and the second and third steps above are repeated until a complete new generation is produced. Once this is achieved, parallel processing is used to increase the speed of the genetic algorithm optimization; many simulations are performed concurrently over a network of computers (Koza *et al* 1999).

2.4. Simulation of acoustic propagation

It is vitally important that the acoustic path that is simulated matches the acoustic path studied empirically. Each experimental calvaria is mounted in a stereotactic frame to ensure that it can be rigidly and reproducibly positioned in the hemispherical array described in section 2.2. The positions of the fiducial markers on the frames can be measured relative to the hemispherical ultrasound transducer using a 3D Cartesian calibrated positioning system. By identifying these same fiducial markers in the CT data, it is then possible to determine the geometric solid body transformation from the orientation of the skull in the CT dataset to the orientation of the skull in the experimental apparatus. This transformation can be represented in the classical augmented matrix form

$$\left[\begin{array}{ccc|c} \vdots & & & \vdots \\ \cdots & \mathbf{R} & \cdots & \mathbf{T} \\ \vdots & & & \vdots \\ \hline 0 & 0 & 0 & 1 \end{array} \right] \quad (3)$$

where \mathbf{R} is a 3×3 matrix describing rotation of the skull and \mathbf{T} is a 3-element vector describing translation of the skull. The determinant of \mathbf{R} is necessarily unity as we require a solid body transformation since the skull does not change in size. A minimum of three fiducial markers that are not colinear is required, although the fidelity of this transformation is improved by using more markers. Determining the optimum values of \mathbf{R} and \mathbf{T} for arbitrarily many fiducial markers is an over-determined problem; fortunately Horn (1986) developed an elegant closed-form solution in quaternions for determining orientation in visual systems that is mathematically equivalent to this problem. There is a unique correspondence between a solid body transformation and its quaternion. A typical 3D computer reconstruction of the skull CT data coupled with a 500-element hemispherical array is shown in figure 3.

As the bones of the skull are heterogeneous, an algorithm is required that is capable of simulating acoustic propagation in a material with rapidly changing local acoustic properties.

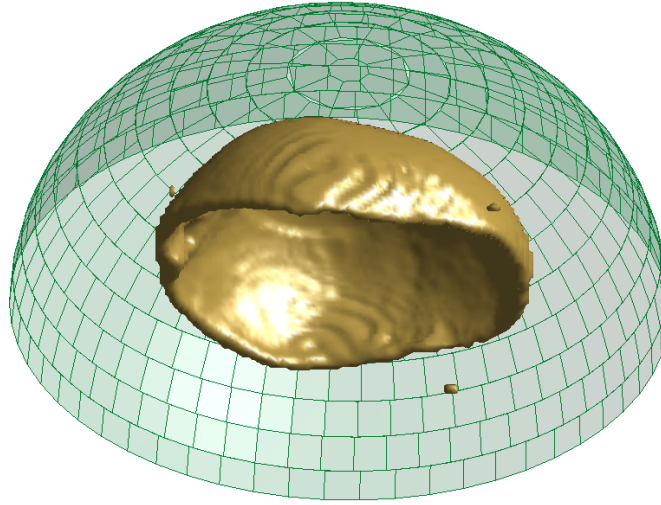


Figure 3. A computer reconstruction of a human calvarium showing its positioning within a hemispherical transducer.

Acoustic propagation is simulated using a FDTD algorithm based on the following formulation of the Westervelt equation (Westervelt 1963):

$$\frac{\partial^2 p}{\partial z^2} - \frac{1}{c^2} \frac{\partial^2 p}{\partial t^2} + \frac{\delta}{c^4} \frac{\partial^3 p}{\partial t^3} + \frac{2\beta}{\rho c^4} \left[p \frac{\partial^2 p}{\partial t^2} + \left(\frac{\partial p}{\partial t} \right)^2 \right] - \frac{\partial p}{\partial z} \cdot \frac{\partial(\ln \rho)}{\partial z} = 0 \quad (4)$$

where p is the pressure of the acoustic wave, ρ is the local density, δ is the local acoustic diffusivity, β is the coefficient of nonlinearity and c is the local speed of sound.

The local density at a particular point is generated from the CT scan of the calvarium. CT scans return data as HU rather than as density. This problem can be overcome by ensuring that a sample of both water and air appear in the CT scan. Since the densities of water and air can be reasonably taken to be 1000 kg m^{-3} and 0.0 kg m^{-3} , respectively, a linear normalization relation can be produced where

$$\kappa_1 = \frac{1}{H_{\text{water}} - H_{\text{air}}} \quad \kappa_0 = \frac{-\overline{H_{\text{air}}}}{H_{\text{water}} - H_{\text{air}}} \quad (5)$$

and thus for any particular point we state that

$$\rho_{\text{ct}} = \kappa_1 \text{HU} + \kappa_0 \quad (6)$$

where ρ_{ct} is the apparent local density in kg m^{-3} based on the CT scan, and κ_1 and κ_0 are constants with units of kg m^{-3} , HU^{-1} and kg m^{-3} , respectively.

For harmonic excitation, $\delta = \frac{2\alpha c^3}{(2\pi f)^2}$ where α is the acoustic amplitude attenuation coefficient and f is the frequency of the ultrasound wave. As stated in section 2.2, here $f = 0.74 \text{ MHz}$ to harness the skull acoustic window. While a precise consensus on the amplitude attenuation coefficient is not available from the literature, a value of $\alpha = 167 \times \frac{f}{10^6} \text{ Np m}^{-1}$ for cortical bone and $\alpha = 300 \times \frac{f}{10^6} \text{ Np m}^{-1}$ for trabecular bone is consistent (Fry and Barger 1978, Theismann and Pfander 1949, Martin and McElhaney 1971). In order to decide which α value should be used, we use the guideline that trabecular bone may be considered to be that bone structure which is composed of 70% or less bone matrix (Gibson and Ashby 1997). Cortical bone in bulk has a density of approximately 1950 kg m^{-3} (Fry and Barger 1978,

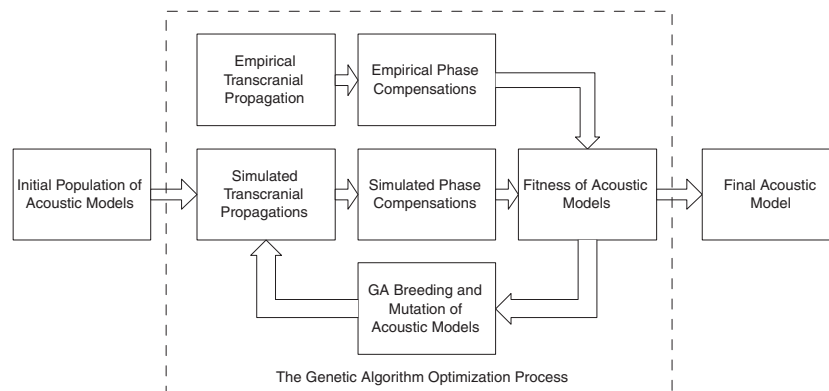


Figure 4. Block diagram of the genetic algorithm optimization of speed-of-sound model.

Abendschein and Hyatt 1970), so for the purposes of absorption we assign the higher value of α to bone with $\rho_{ct} < (0.7 \times 1950 + 0.3 \times 1000) \text{ kg m}^{-3}$, i.e., $\rho_{ct} < 1665 \text{ kg m}^{-3}$.

The value of the nonlinear parameter β is set to zero, effectively simulating linear acoustic propagation. The pressure amplitude of the ultrasound used empirically is sufficiently low for nonlinear acoustic effects to be negligible; the Goldberg number Γ is also expected to be small due to the high attenuation α (Blackstock 1964). Furthermore, the value of β in bone has not yet been satisfactorily determined.

Discretization parameters Δt and Δz are chosen to ensure numerical stability in the simulation. This requirement is enforced by requiring the Courant–Friedrichs–Levy (CFL) number to be less than or equal to unity at all points, where $\text{CFL} = c\Delta t/\Delta z$ (Taflove 1995).

2.5. The complete method by action

A genetic algorithm optimization structured as the block diagram in figure 4 provides a robust method for determining an appropriate speed-of-sound model. The method is precisely defined as the following steps:

1. The calvarium of a human skull is placed within a stereotactic positioning frame and scanned at high resolution using a clinical CT scanner (Siemens Somatom Plus 4, Kernel AH-82).
2. A 500-element hemispherical ultrasound transducer is placed in a baffled tank filled with degassed and deionized water. A needle hydrophone is placed at the geometric centre of the transducer.
3. A random selection of 40 elements is made from the 500 elements of the hemispherical ultrasound transducer.
4. Each selected element is activated in turn and the phase of the ultrasound received at the hydrophone is recorded, giving the phase shift between the transducer and the hydrophone in water alone.
5. The calvarium is mounted between the transducer and the hydrophone using the stereotactic apparatus so that the relative alignment of the transducer, skull and hydrophone can be determined, and repeatedly established.
6. The 40 selected elements are again activated in turn and the phase of the ultrasound received at the hydrophone is recorded. The differences between the phase measurements without and with skull present are calculated.

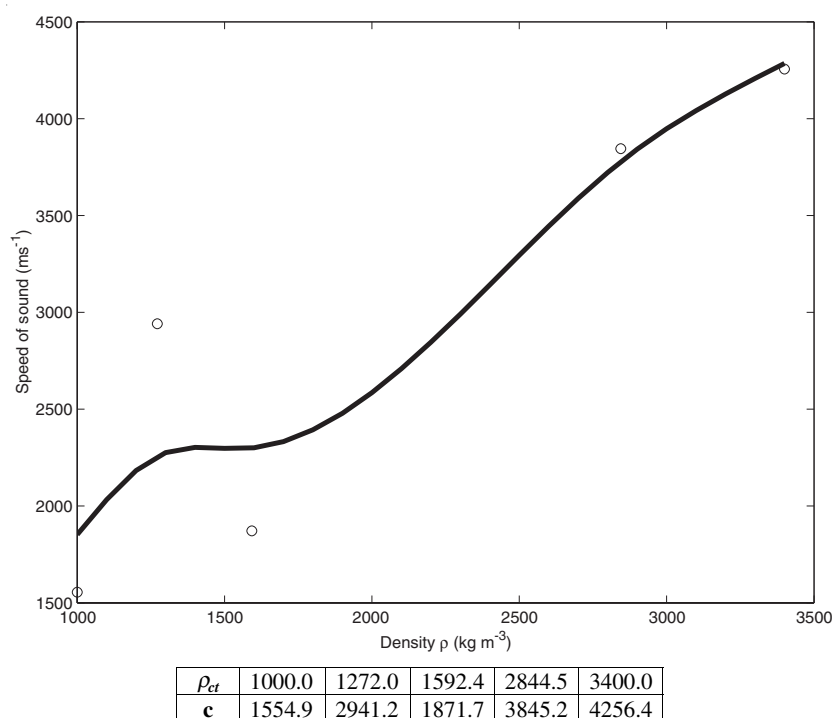


Figure 5. The final model for speed of sound in cranial bone based on apparent density by CT scan.

7. A 3D model of the skull is reconstructed computationally and the CT data in HUs is normalized to apparent density. The alignment between the transducer and stereotactically mounted skull is calculated.
8. The acoustic propagation is computationally simulated given a certain model of acoustic velocity in skull bone. The phase changes predicted by simulation are compared against the empirically measured phase changes.
9. This process is repeated across four skulls and for 50 initial speed-of-sound models.
10. The next generation of 50 speed-of-sound models are evolved using the principles of genetic algorithm optimization, namely selection, mutation and crossover, as elaborated in section 2.3 (Holland 1975, Goldberg and Deb 1991).
11. The process is repeated for 50 generations.
12. The best speed-of-sound model is chosen by selecting the model that has produced the best phase correlation metric as defined in section 2.3.

3. Results

Ultimately, after 50 generations, the model shown in figure 5 was produced for the speed of sound against apparent bone density by CT scan. This model is stated in numerical form in table 1.

3.1. Statistical significance in phase correlation measurements

Since the speed-of-sound model generated in this paper was produced by its ability to generate correctly model phase shifts across skull, the null hypothesis for this study is that the model

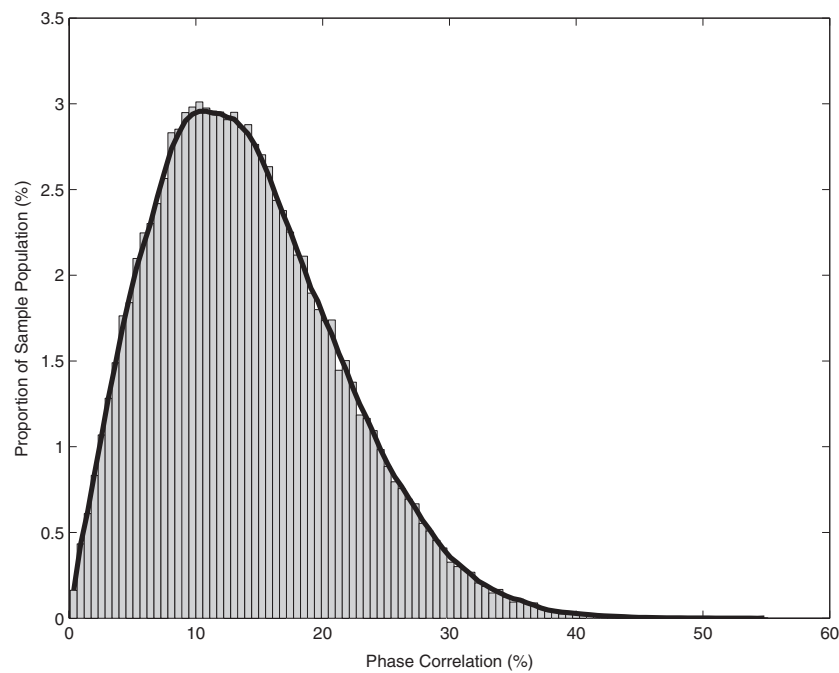


Figure 6. The probabilistic distribution of the phase correlation metric for randomly assigned phases.

Table 1. Speed of sound in cranial bone as a function of apparent bone density by CT scan in intervals of 100 kg m^{-3} .

$\rho_{ct} \text{ (kg m}^{-3}\text{)}$	$c \text{ (m s}^{-1}\text{)}$	$\rho_{ct} \text{ (kg m}^{-3}\text{)}$	$c \text{ (m s}^{-1}\text{)}$
1000	1852.7	2300	2991.1
1100	2033.0	2400	3142.1
1200	2183.8	2500	3294.6
1300	2275.8	2600	3444.7
1400	2302.6	2700	3588.5
1500	2298.1	2800	3722.2
1600	2300.3	2900	3841.9
1700	2332.5	3000	3947.6
1800	2393.4	3100	4041.9
1900	2479.0	3200	4127.7
2000	2585.4	3300	4207.8
2100	2708.8	3400	4285.1
2200	2845.3		

produces no better correlation between simulation and empirical data than would be produced by choosing the modelled phase shifts randomly.

To determine whether the speed-of-sound model is statistically significant, it is first necessary to characterize the distribution of randomly chosen phase shifts. This distribution is shown in figure 6, and is based upon 100 000 trials of sets of 40 randomly generated phase shifts.

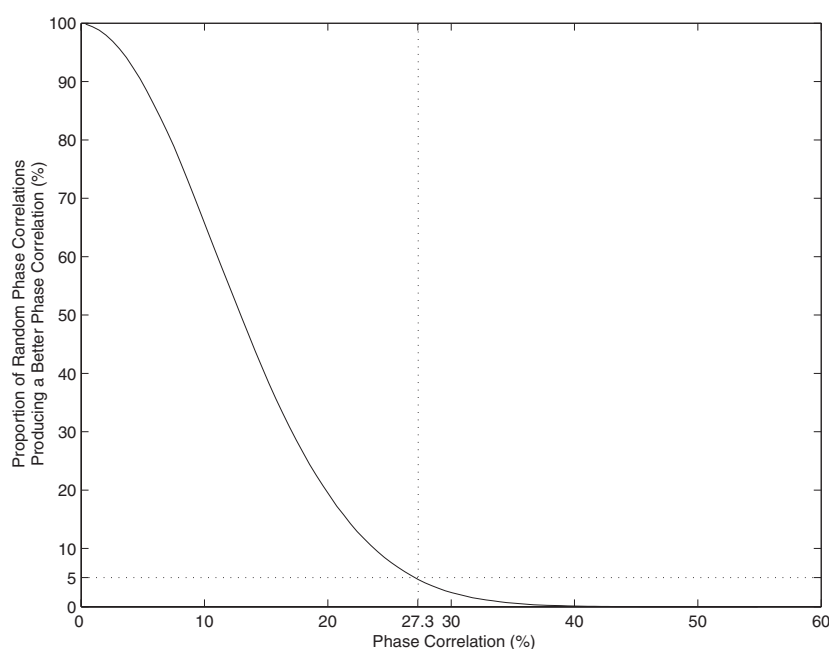


Figure 7. Statistical significance curve for the phase correlation metric.

A statistical significance curve as shown in figure 7 can then be calculated. For a given phase correlation value, this curve gives the proportion of random phase assignments that would be expected to produce a better phase correlation. Only 5% of random phase assignments would be expected to produce a better phase correlation value than 27.3%, and thus a model that is capable of producing phase correlations better than 27.3% is statistically significant at $p < 0.05$ from the point of the view of the null hypothesis described above.

In fact, the best speed-of-sound model generated by the genetic algorithm produced a phase correlation value of 53.4%, and is therefore very highly significant. Previous work in the literature of speed of sound of models for bone includes an interesting model proposed by Clement and Hynynen (2002a) based upon assigning an effective speed of sound to a region of skull based on an average of the densities in that region obtained by CT scan (Clement and Hynynen 2002a). The relationship between effective speed of sound and density in Clement and Hynynen (2002a) is

$$c_{\text{eff}} = 2.06\bar{\rho} - 1540 \quad (7)$$

where c_{eff} is in m s^{-1} and ρ is in kg m^{-3} . When applied to the data in this study, this model produced a phase correlation value of 49.2%; it is therefore outperformed here by the speed-of-sound model produced by genetic algorithm. The result of 49.2% is also very highly statistically significant by the method described above.

3.2. Comparison of the genetic algorithm speed-of-sound model to a speed-of-sound model based on the homogenization of skull

This paper describes the production of a general model for the speed of sound in skull, based upon the analysis of a finite number of experimental calvaria. This problem is therefore of the class of problems where an optimization process is used to produce a generally applicable result

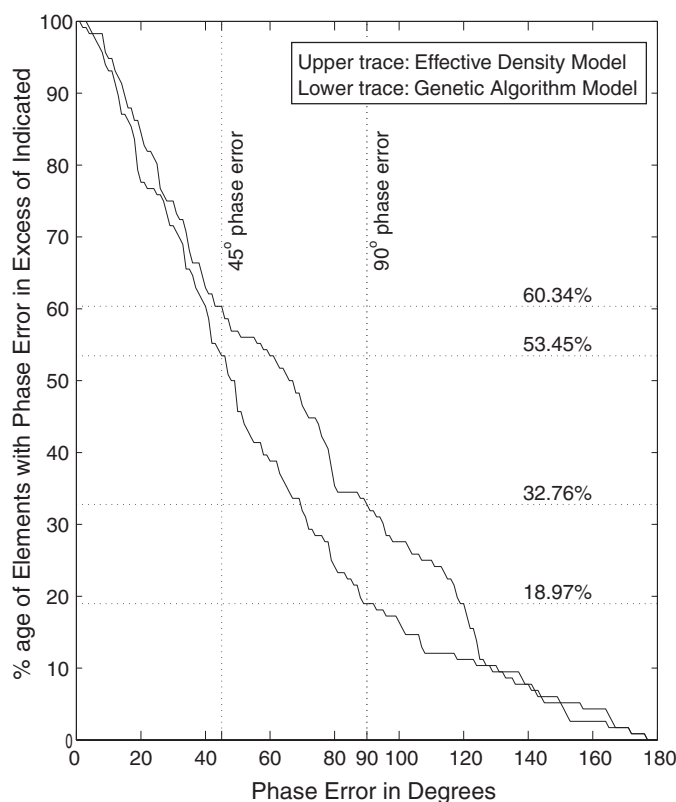


Figure 8. Comparison of the performance of the linear speed model and the genetic algorithm speed model for a skull not used in the optimization process.

from a pool of empirical data. Therefore, it must be established that the genetic algorithm has general applicability by using it in the analysis of ultrasound propagation through a calvarium that was not used in the optimization procedure. This is necessary to show that the optimization is not over-trained; over-training occurs when an algorithm performs well on members of the original dataset against which it was formed, but performs very badly on novel datasets.

An unused calvarium was placed in the same experimental apparatus as described in section 2.2 above, and the phase shifts due to transcranial propagation of the ultrasound were measured in 116 elements corresponding to the top 6 layers of the 500-element hemispherical array as shown in figure 3. The top six layers were chosen because elements chosen near the rim of the transducer in this experimental configuration may have greater accessory pathways to the focus point through water without impinging on skull, as may be inferred from figure 3. Choosing the elements that comprise the top 6 layers of the transducer gives a representative number of elements over which to compare the two models while also ensuring transcranial propagation to the focus. Ultrasound propagation was modelled using the FDTD algorithm described in equation (4). However, two simulations were run: the first simulation used the effective density speed-of-sound model (Clement and Hynynen 2002a) as shown in equation (7), and the second simulation used the speed-of-sound model derived in this paper by genetic algorithm optimization as shown in figure 5 and table 1.

The distribution of θ_e (as defined in section 2.3) for each of the two speed-of-sound models is shown for this novel calvarium in figure 8. These curves show the proportion of

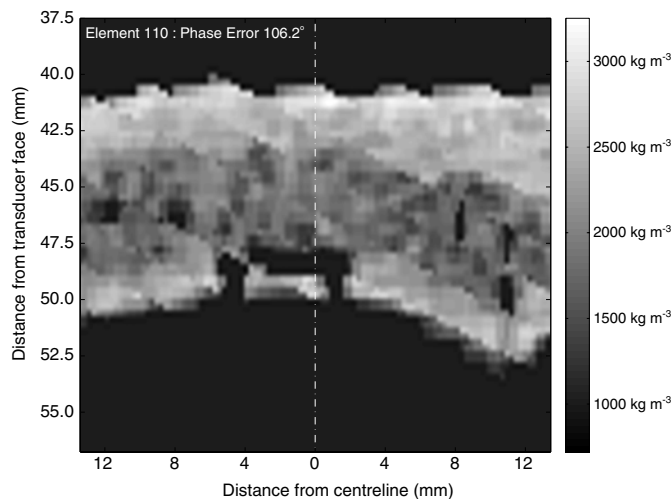


Figure 9. CT cross section showing an instance of complex lacunar structure.

elements that have a θ_e greater than a particular error margin; all curves must begin at 100% at $\theta_e = 0^\circ$ and end at 0% at $\theta_e = 180^\circ$. Better algorithms have traces that run lower on the graph. The genetic algorithm speed-of-sound model outperforms the effective density speed-of-sound model across the range of θ_e . In particular, it is apparent that the effective density model suffered by having over 30% elements with $\theta_e > 90^\circ$, which counts poorly in the phase correlation metric $\cos \theta_e \times 100\%$ as defined in section 2.3.

The effective density model produced a phase correlation metric of 28.36%. The genetic algorithm speed-of-sound model, however, produced a phase correlation metric of 44.8%, which is markedly better when judged in light of the statistical analysis given above in section 3.1. Furthermore, this result is of a broadly equivalent level of performance to that seen with the calvaria used in the optimization procedure, and as such refutes the presence of substantial over-training in the speed-of-sound model.

The presence of elements with $\theta_e > 90^\circ$ with the genetic algorithm speed-of-sound model appears to be due primarily to anomalies in the material geometry of the skull that are not well analysed by the comparatively simple one-dimensional (1D) FDTD model described in equation (4). In particular, these errors tend to arise when complex lacunae are present in the simulation; figure 9 shows a portion of the CT data for such a case where a substantial lacuna is present in the inner table of the calvarium along the simulation path. Of the elements with $\theta_e > 90^\circ$ with the genetic algorithm speed-of-sound model, 73% had readily apparent lacunae on the simulation path on inspection. Ideally the genetic algorithm optimization would be conducted with a full 3D simulation of acoustic propagation. However, even using suitable distributed computing techniques to perform the optimization in this way with an equivalent population of speed models and number of generations might be expected to have taken several years with the currently available computing power. Consequently, a full 3D treatment is not possible at this time.

4. Discussion

This paper describes a novel method for establishing a model of the speed of sound in cranial bone. An important difference from previous work is that this method produces a model for the speed of sound at any particular point in the skull; the model is not dependent on

dividing the cranial bone into regions or layers, or on ascribing homogenized properties to any part of the skull. This model is valid for cranial bone of both cortical and trabecular structure, and is based on a coupled strategy of genetic algorithm optimization of CT-based acoustic simulation and empirical measurement of the change in phase of an ultrasound wave on transmission through human calvaria.

The paper also details the results of this novel method in the form of a model for the speed of sound in cranial bone dependent on local density as shown in figure 5 and as described in section 3, and further establishes the statistical significance of this result and compares its performance to another speed-of-sound model in the literature Clement and Hynynen (2002a). As indicated in the introduction, this improvement in the characterization of the acoustic properties of cranial bone is necessary for the development of non-invasive transcranial focused ultrasound surgery.

Non-invasive transcranial focused ultrasound surgery requires precise *a priori* prediction of the distortion introduced into the acoustic field by the presence of the skull; this distortion cannot be determined without a thorough knowledge of the geometry of the skull and its acoustic properties. The distribution of the speed of sound in the skull is the most important of these acoustic properties since it most affects the phase of the transmitted ultrasound wave.

The modelling process described in this paper makes certain assumptions about the nature of trabecular orientation in cranial bone, the use of CT data to provide apparent density measurements and the use of phase measurements as a basis for optimization; these assumptions and the justifications for their use are discussed below. The speed-of-sound model produced in this paper is then compared to prior notable work on entirely homogeneous models for the speed of sound in skull bone (Fry and Barger 1978, Theismann and Pfander 1949, Martin and McElhaney 1971, Duck 1990).

4.1. Trabecular orientation

The speed-of-sound model derived in this paper is expressed in the form $c(\rho_{ct})$, which implicitly disregards the direction of propagation of the ultrasound wave. Some studies (Lees *et al* 1983, Nicholson *et al* 1994, McCarthy *et al* 1990) have found marked anisotropy in the speed of sound of ultrasound in bone, which would require a model of the form $c(\rho_{ct}, \underline{u})$ with \underline{u} as the vectorial direction of propagation. However, these studies have been performed in such bones as the calcaneus, long bones of the leg or vertebral bodies—in these cases, the bone is clearly placed under a predominant mechanical loading which gives rise to an equivalent orientation in the trabecular lattice. Faster acoustic propagation is found where \underline{u} is parallel to the direction of mechanical loading; this faster propagation velocity is accounted for by acoustic bar wave propagation directly down the trabecular framework and is not strongly correlated to the density of the bone (Nicholson *et al* 1994). In contrast, cranial bone is self-evidently not placed under routine directional loading, and so there is little mechanical stimulus towards any particular trabecular orientation (White 1986). Furthermore, transcranial acoustic propagation places stringent requirements on the range of permissible propagation directions; the high level of acoustic absorption in skull requires that the direction of propagation be close to normal to the surface of the skull to shorten the path in bone and hence permit a sufficiently intense intracranial acoustic field to be developed. As described earlier, the direct wave strongly dominates in transmission through the skull for angles of incidence within 20° of normal (Hayner and Hynynen 2001) and therefore the effect of \underline{u} on the production of the shear mode of acoustic propagation may be neglected.

The model used in the genetic algorithm optimization process also does not include any special treatment of potential ultrasound scattering in trabecular bone. However, Chaffai *et al*

(2000) have already treated this matter, in which it was found that ‘at frequencies less than 1 MHz (the clinically useful frequencies), no broadening of the transmitted pulse temporal profile, apart from the effect of the frequency dependent attenuation, has been evidenced’ and that ‘for the time being, experiments do not suggest the presence of strong multiple scattering’.

Given these practical constraints on \underline{u} for acoustic use and the non-orientation of the cranial trabecular framework, the $c(\rho_{ct})$ formulation is sufficient.

4.2. Generalization of apparent density

The model described here is based on ρ_{ct} , since in patient studies only the apparent density obtained from the CT scan could be expected to be available. However, this leaves the question of whether this apparent density is suitably close to the true density of the material. The use of anatomic specimens of human calvaria in this study allows us to address this question by examining the effect of one further simple constraint on the conversion of HUs to CT data; we may require that the sum of the apparent densities of all CT points identified as being skull bone multiplied by the volume of a voxel of CT data be equal to the empirically measurable mass of the calvarium. A quadratic conversion between HUs and skull density can then be established based on this mass requirement, the density of air and the density of water. The correlation between this quadratic conversion and the original linear conversion provides an estimate of the reasonableness of using ρ_{ct} and also allows the $c(\rho_{ct})$ model to be generalized to other methods of acquiring bone density information.

Given a calvarium of mass M , therefore

$$M = \int \int \int_{\text{skull}} \rho \cdot dV \cong \sum_{\text{skull}} \rho \cdot \Delta V \quad \Rightarrow \quad \frac{M}{v} = \sum_{\text{skull}} \rho \quad (8)$$

where v is the volume of a voxel of CT data. Now, using a quadratic conversion of HUs

$$\begin{aligned} \frac{M}{v} &= \sum_{\text{skull}} (\kappa_2 \text{HU}^2 + \kappa_1 \text{HU} + \kappa_0) \\ \Rightarrow \quad \frac{M}{vn_{\text{skull}}} &= \left[\frac{1}{n_{\text{skull}}} \sum_{\text{skull}} \text{HU}^2 \quad \frac{1}{n_{\text{skull}}} \sum_{\text{skull}} \text{HU} \right] [\kappa_2 \ \kappa_1 \ \kappa_0] \end{aligned} \quad (9)$$

where n_{skull} is the number of voxels identified as representing the calvarium, and κ values are parameters of the quadratic conversion. The parameters of the conversion can then be established by solving the following relationship:

$$\begin{bmatrix} \frac{1}{n_{\text{air}}} \sum_{\text{air}} \text{HU}^2 & \frac{1}{n_{\text{air}}} \sum_{\text{air}} \text{HU} & 1 \\ \frac{1}{n_{\text{water}}} \sum_{\text{water}} \text{HU}^2 & \frac{1}{n_{\text{water}}} \sum_{\text{water}} \text{HU} & 1 \\ \frac{1}{n_{\text{skull}}} \sum_{\text{skull}} \text{HU}^2 & \frac{1}{n_{\text{skull}}} \sum_{\text{skull}} \text{HU} & 1 \end{bmatrix} \begin{bmatrix} \kappa_2 \\ \kappa_1 \\ \kappa_0 \end{bmatrix} = \begin{bmatrix} \rho_{\text{air}} \\ \rho_{\text{water}} \\ \frac{M}{vn_{\text{skull}}} \end{bmatrix} \quad (10)$$

where n_{air} and n_{water} are the number of voxels identified as representing air and water. This solution method may be extended over any number of CT scans of different calvaria by adding further lines to the relationship given above using the appropriate M , HU and n_{skull} values in each case. The resulting system of equations is over-determined but may be solved for the best values of the κ parameters using the standard least-squares metric; the rows of the linear system should be normalized to account for the different values of n_{air} , n_{water} and n_{skull} to prevent unacceptable weighting of the solution in the least-squares method. Based on the calvaria used in this study we find κ parameters of $[\kappa_2 \ \kappa_1 \ \kappa_0] = [-8.837 \times 10^{-5} \ 1.092 \ -36.8]$, which is very nearly linear over our region of interest.

4.3. Limits on phase-based inference of speed-of-sound models

Since this speed-of-sound model is based on the optimization of phase-shift information, it is appropriate to enquire whether this model might be skewed by this method. Phase-shift information may only take values between 0 and 2π radians since phase is periodic by definition. Consequently, it is not possible to distinguish a phase shift of ϕ radians from a phase shift of $\phi + 2\pi$ radians since they are obviously identical modulo 2π . This is a problem of wrapping in phase.

If we consider the assigning of a particular speed of sound to a particular local density, this problem of phase wrapping might occur if the true speed of sound for that local density was sufficiently different from the speed of sound in the model. We can estimate the limits of this problem by calculating the size of error in the speed of sound required to produce this phase wrapping uncertainty.

Given an ultrasound frequency of f , a material thickness of x and a speed of sound of c_0 , the phase shift ϕ across the material would be expected to be

$$\phi = \frac{2\pi f x}{c_0}. \quad (11)$$

The limits we seek are the increase and decrease in c_0 necessary to produce a phase shift of π in the predicted phase

$$\phi + \pi = \frac{2\pi f x}{c_0 - \Delta c_{\text{low}}} \quad \phi - \pi = \frac{2\pi f x}{c_0 + \Delta c_{\text{high}}}. \quad (12)$$

By re-arrangement, the following limits can therefore be established:

$$\Delta c_{\text{low}} = c_0 - \frac{2c_0 f x}{2f x + c_0} \quad \Delta c_{\text{high}} = \frac{2c_0 f x}{2f x - c_0} - c_0. \quad (13)$$

Thus, if the model speed of sound is c_0 , but the true speed of sound is $c_0 + \Delta c_{\text{high}}$, this will produce the same phase-shift information as if the true speed of sound were $c_0 - \Delta c_{\text{low}}$. Fortunately these limits are wide enough, as shown in figure 10, for this problem not to occur in practice in this optimization.

4.4. Comparison to other prior work

Bone, in its cortical and trabecular forms, may be considered to be a form of cellular solid. Cellular solids are those materials that are composed of a material lattice, that latticework forming either open or closed pores (Gibson and Ashby 1997).

The most straightforward model for speed of sound in a material is

$$c = \sqrt{\frac{E}{\rho}} \quad (14)$$

where E is the Young's modulus of the material and ρ its density. However, for open-pore cellular materials it can be shown that $E \propto \rho^2$ and that for closed-pore materials $E \propto \rho^3$ (Gibson and Ashby 1997).

This curve of speed of sound against bone density obtained in our study has a form in keeping with these theoretical material properties of skull. Initially, it has a form similar to that of a square root function of speed against density for an open-celled porous solid, as would be the case for low volume fraction trabecular bone. The model transitions into a linear region in keeping with the material structure of dense cortical bone. The transitional region is between 1665 kg m^{-3} , the upper limit for the density of bulk trabecular bone based upon the 70% bone volume fraction requirement and 1950 kg m^{-3} , the density for the bulk of cortical bone.

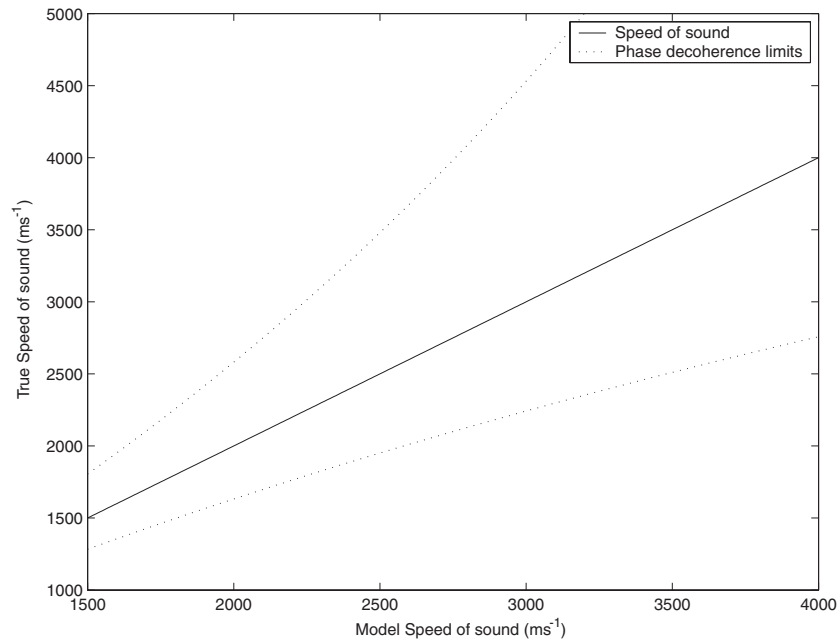


Figure 10. Speed of sound limits in phase based optimization.

Using the values of ρ_{ct} for the calvaria in this study, the distribution of c in each calvarium can be calculated based on the model we have described. An appropriate average of the distribution of c provides a basis for comparison with pre-existing measurements of the speed of sound in bone.

The most appropriate average for the distribution of c is not the simple arithmetic mean of c . If we consider a very simple model for the propagation of a wave through some heterogeneous material, the time taken for the wave to travel through the material t is

$$t = \int \frac{1}{c(x)} \delta x. \quad (15)$$

Now if the material has thickness x then the average speed of sound c_{av} through the material becomes

$$c_{av} = \frac{x}{t} = x \left(\int \frac{1}{c(x)} \delta x \right)^{-1} \quad (16)$$

and so

$$c_{av} = (\overline{c^{-1}})^{-1} \quad (17)$$

where $\overline{c^{-1}}$ is the arithmetic mean of the distribution of the reciprocal of c . Calculating for the four calvaria here, bulk c_{av} speeds of sound of 2609.9 m s^{-1} , 2884.8 m s^{-1} , 2829.9 m s^{-1} and 2756.8 m s^{-1} can be found. These values are entirely in keeping with the range of values seen in the current literature (Fry and Barger 1978, Theismann and Pfander 1949, Martin and McElhaney 1971, Duck 1990).

5. Conclusion

The genetic algorithm optimization method coupled to acoustic simulation and experimental phase measurements provides a useful method for determining the variation in speed of sound in cranial bone with density. The model produced in this paper using this method has been shown to predict the speed of sound in transcranial propagation better than pre-existing homogenized speed of sound methods. Finally, it must be cautioned that the model in this paper is based on measurements of the acoustic properties of a limited number of formalin-preserved human cadaveric skulls and therefore it cannot be safely assumed without further study that the model is representative of the entire population of human skulls or of *in vivo* transcranial propagation.

Acknowledgment

Supported by NIH grant CA76550.

References

- Abendschein W and Hyatt G W 1970 Ultrasonics and selected physical properties of bone *Clin. Orthop.* **69** 294–301
- Antonisse J 1989 A new interpretation of schema notation that overturns the binary encoding constraint *Proc. 3rd Int. Conf. on Genetic Algorithms* pp 86–91
- Averkiou M A and Cleveland R O 1999 Modeling of an electrohydraulic lithotripter with the KZK equation *J. Acoust. Soc. Am.* **106** 102–12
- Blackstock D T 1964 Thermoviscous attenuation of plane, periodic, finite-amplitude sound waves *J. Acoust. Soc. Am.* **36** 534–42
- Chaffai S, Roberjot V, Peyrin F, Berger G and Laugier P 2000 Frequency dependence of ultrasonic backscattering in cancellous bone: autocorrelation model and experimental results *J. Acoust. Soc. Am.* **108** 2403–11
- Chapelon J Y, Faure P, Plantier M, Cathignol D, Souchon R, Gorry F and Gelet A 1993 The feasibility of tissue ablation using high intensity electronically focused ultrasound *IEEE Ultrasonics Symp.* **93** 1211–4
- Clement G T and Hynynen K 2002a A noninvasive method for focusing ultrasound through the human skull *Phys. Med. Biol.* **47** 1219–36
- Clement G T and Hynynen K 2002b Correlation of ultrasound phase with physical skull properties *Ultrasound Med. Biol.* **28** 617–24
- De Boor C 1978 *A Practical Guide to Splines* (New York: Springer)
- Duck F 1990 Acoustic properties of tissue at ultrasonic frequencies *Physical Properties of Tissue: A Comprehensive Reference Book* (London: Academic)
- Fry F 1979 Transskull transmission of axisymmetric focused ultrasonic beams in the 0.5 to 1 MHz frequency range: implications for brain tissue visualization, interrogation and therapy *Ultrasonic Tissue Characterization* vol 2, ed M Linzer (Washington, DC: National Bureau of Standards) pp 203–8
- Fry F and Barger J 1978 Acoustical properties of the human skull *J. Acoust. Soc. Am.* **63** 1576–90
- Fry F and Johnson L 1978 Tumor irradiation with intense ultrasound *Ultrasound Med. Biol.* **4** 337–411
- Fry W J, Mosberg W, Barnard J W and Fry F J 1954 Production of focal destructive lesions in the central nervous system with ultrasound *J. Neurosurg.* **11** 471–8
- Gibson L J and Ashby M F 1997 *Cellular Solids: Structure and Properties* (Cambridge: Cambridge University Press)
- Goldberg D E and Deb K 1991 A comparative analysis of selection schemes used in genetic algorithms *Foundations of Genetic Algorithms* ed G J E Rawlins (San Mateo, CA: Morgan Kaufmann) pp 69–93
- Greenleaf J F 1986 A graphical description of scattering *Ultrasound Med. Biol.* **12** 603–9
- Hallaj I M and Cleveland R O 1999 FDTD simulation of finite-amplitude pressure and temperature fields for biomedical ultrasound *Acoust. Res. Lett. Online* **1** 7–12
- Hayner M and Hynynen K 2001 Numerical analysis of ultrasonic transmission and absorption of oblique plane waves through the human skull *J. Acoust. Soc. Am.* **110** 3319–30
- Holland J H 1975 *Adaptation in Natural and Artificial Systems* (Ann Arbor, MI: University of Michigan Press)
- Horn B K P 1986 Closed-form solution of absolute orientation using unit quaternions *J. Opt. Soc. Am. A* **4** 629–42
- Hynynen K 1999 Trans-skull ultrasound therapy: the feasibility of using image-derived skull thickness information to correct the phase distortion *IEEE Trans. Ultrason. Ferroelectr. Freq. Control* **46** 752–5

- Hynynen K and Jolesz F A 1998 Demonstration of potential noninvasive ultrasound brain therapy through an intact skull *Ultrasound Med. Biol.* **24** 275–83
- Katz J L 1971 Hard tissue as a composite material: I. Bounds on the elastic properties *J. Biomech.* **4** 455
- Koza J R, Bennett F H, Andre D and Keane M A 1999 Parallelization of genetic programming *Genetic Programming III* (San Mateo, CA: Morgan Kaufmann Publishers) pp 1025–36
- Lakes R, Yoon H S and Katz J L 1985 Ultrasonic wave propagation and attenuation in wet bone *J. Biomed. Eng.* **8** 143–8
- Lees S 1986 Sonic properties of mineralized tissues *Tissue Characterization with Ultrasound* vol 2, ed J F Greenleaf (Boca Raton, FL: CRC Press) pp 207–26
- Lees S, Ahern J M and Leonard M 1983 Parameters influencing the sonic velocity in compact calcified tissues of various species *J. Acoust. Soc. Am.* **74** 28–33
- Lees S, Cleary P F, Heeley J D and Garipey E L 1979 Distribution of sonic plesio-velocity in a compact bone sample *J. Acoust. Soc. Am.* **66** 641–6
- Lele P P 1967 Production of deep focal lesions by focused ultrasound—current status *Ultrasonics* **5** 105–22
- Lele P P and Pierce A D 1973 The thermal hypothesis of the mechanism of ultrasonic focal destruction in organised tissues. Interaction of ultrasound and biological tissues *FDA 73–8008 BRH/DBE* (Washington, DC: Bureau of Radiological Health) pp 121–8
- Lizzi F L, Coleman D J, Driller J, Ostromogilsky M, Chang S and Greenall P 1984 Ultrasonic hyperthermia for ophthalmic therapy *IEEE Trans. Sonics Ultrason.* **31** 473–81
- Lynn J G and Putnam T J 1944 Histology of cerebral lesions produced by focused ultrasound *Am. J. Pathol.* **20** 637–52
- Lynn J G, Zwemer R L, Chick A J and Miller A E 1942 A new method for the generation and use of focused ultrasound in experimental biology *J. Gen. Physiol.* **26** 179–93
- Martin B and McElhaney J H 1971 The acoustic properties of human skull bone *J. Biomed. Mater. Res.* **5** 325–33
- McCarthy R N, Jeffcott L B and McCartney R N 1990 Ultrasound speed in equine cortical bone: effects of orientation, density, porosity and temperature *J. Biomech.* **23** 1139–43
- Nicholson P H F, Haddaway M J and Davie M W J 1994 The dependence of ultrasonic properties on orientation in human vertebral bone *Phys. Med. Biol.* **39** 1013–24
- Poloni C and Pediroda V 1998 GA coupled with computationally expensive simulations: tools to improve efficiency *Genetic Algorithms and Evolution Strategies in Engineering and Computer Science* ed D Quagliarella, J Periaux, C Poloni and G Winter (Chichester: Wiley) pp 267–88
- Sanghvi N T, Fry F, Bihle R, Foster F S, Phillips M H, Syrus J, Zaitsev A V and Hennige C W 1996 Noninvasive surgery of prostate tissue by high-intensity focused ultrasound *IEEE Trans. Ultrason. Ferroelectr. Freq. Control* **43** 1099–110
- Shaffer R E and Small G W 1996 Genetic algorithms for the optimization of piecewise linear discriminants *Chemometr. Intell. Lab. Syst.* **35** 87–104
- Sun J and Hynynen K H 1998 Focusing of therapeutic ultrasound through a human skull: a numerical study *J. Acoust. Soc. Am.* **104** 1705–15
- Sun J and Hynynen K H 1999 The potential of transskull ultrasound therapy and surgery using the maximum available skull surface area *J. Acoust. Soc. Am.* **105** 2519–27
- Taflove A 1995 *Computational Electromagnetics: The Finite-Difference Time-Domain Method* (Boston, MA: Artech House Publishers)
- Tanter M, Aubry J F, Gerber J, Thomas J L and Fink M 2001 Optimal focusing by spatio-temporal inverse filter: I. Basic principles *J. Acoust. Soc. Am.* **110** 37–47
- Tanter M, Thomas J L and Fink M 1998 Focusing and steering through absorbing and aberrating layers: application to ultrasonic propagation through the skull *J. Acoust. Soc. Am.* **103** 2403–10
- ter Haar G R, Sinnott D and Rivens I 1989 High intensity focused ultrasound—a surgical technique for the treatment of discrete liver tumors *Phys. Med. Biol.* **34** 1743–50
- Theismann H and Pfander F 1949 Uber die Durchlassigkeit des Knochens fur Ultraschall *Strahlentherapie* **80** 607–10
- Westervelt P J 1963 Parametric acoustic array *J. Acoust. Soc. Am.* **35** 535–7
- White D N 1986 The acoustic characteristics of skull *Tissue Characterization with Ultrasound* vol 2, ed J F Greenleaf (Boca Raton, FL: CRC Press) pp 1–39
- Wright A H 1991 Genetic algorithms for real parameter optimization *Foundations of Genetic Algorithms* ed G J E Rawlins (San Mateo, CA: Morgan Kaufmann) pp 205–18